Summer Student Report

Prospects for the Measurement of the Total Decay Width of the Higgs Boson at the International Linear Collider

Tom Hadavizadeh
University of Cambridge
th390@cam.ac.uk
Supervisor: Claude Fabienne Dürig

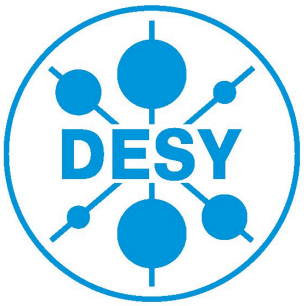

FLC Group

DESY

September 4, 2013

Abstract

A full simulation of the total decay width of the Higgs Boson at the ILC was carried out to investigate how large the uncertainty on the measurement is expected to be. The simulation was carried out at a centre of mass energy of $\sqrt{s} = 500$ GeV and luminosity of $\mathcal{L} = 500$ fb^{-1}. The total decay width was investigated indirectly by looking at the WW fusion formation process and the $H \to b\bar{b}$ decay process. By applying selection cuts the background and Higgs strahlung processes were removed and a fit was used to obtain the uncertainty on the number of WW fusion events. By using the error in the branching ratios of $H \to b\bar{b}$ and $H \to WW$ the uncertainty in the total decay width was established to be $\left(\frac{\Delta\Gamma_H^{tot}}{\Gamma_H^{tot}}\right) = 2.8\%$ which is consistent with previous fast simulations.

Contents

1 Introduction

In this report I will give a record of the project I have undertaken as part of the DESY Summer Student Programme. I have worked as part of the FLC group *(Forschung mit Leptoncollidern)* under the supervision of Claude Fabienne Dürig. This project aims to determine the total decay width of the Higgs Boson by running simulations for the proposed International Linear Collider *(ILC)*.

On the 4th July 2012 the two experiments ATLAS and CMS which operate at the Large Hadron Collider in CERN released data that confirmed a Higgs-like particle had been found to a 5σ level. The ILC is designed to make precision measurements and will be used to establish the properties of this particle. I will give a summary of the relevant theoretical background in section 2. Here there will be a general overview of the standard model predictions for the Higgs Boson and details of its production and decay.

In section 3 I will define the signal process that I am looking to isolate as well as the processes that add to the background and should be removed. In section 4 I will detail the specific cuts applied to the data sets in order to keep the signal events and remove the background. I will also illustrate how it is possible to obtain the total decay width from the signal events used. There will be a summary of my findings in section 5 where I will conclude what I have found.

This analysis is conducted at a centre of mass energy $\sqrt{s} = 500\,\text{GeV}$, the full energy of the ILC. This is also assumes an integrated luminosity of $\mathcal{L} = 500\ \text{fb}^{-1}$ and a Higgs mass of $m_H = 125\,\text{GeV}$.

2 Theory

2.1 The Standard Model

The Standard Model is a theory that incorporates the electromagnetic, weak, and strong interactions that control the dynamics of the elementary particles. These particles comprise of leptons and quarks, which are both fermions and shown in table 1, and gauge bosons as shown in table 2.

Generation	**Quarks**		**Leptons**	
1	u	d	ν_e	e
2	c	s	ν_μ	μ
3	t	b	ν_τ	τ
Charge Q/ $\lvert e \rvert$	$+\frac{2}{3}$	$-\frac{1}{3}$	0	-1

Table 1: *Elementary Fermions*

The quarks interact with the strong, weak and electromagnetic forces where as the leptons carry no color charge so can not interact via the strong force. Each of the particles in table 1 have a corresponding antiparticle with the same mass and opposite charge.

The gauge bosons mediate the interactions between the particles and they arise as a result of local gauge invariance. This requirement means the standard model can be written as the gauge group $SU(3)_C \times SU(2)_L \times U(1)_Y$. The label of each group represents the charges of the interactions: C is colour for the strong force, L is the left-handed isospin in the weak interaction, and Y is the hypercharge for electromagnetic interactions. These gauge bosons are listed in table 2 along with some of their properties.

Interaction	**Name**	**Symbol**	**Charge** Q/ $\lvert e \rvert$	**Mass** Gev/ c^2
Electromagnetic	photon	γ	0	0
Strong	gluon	g	0	0
Weak		$W^{\pm}$, Z	± 1, 0	80.4, 90.2

Table 2: *Gauge Bosons*

Local gauge invariance requires that the bosons that mediate the forces are massless, but in reality the $W^{\pm}$ and Z bosons have mass. This results via the *Higgs Mechanism* where the symmetry of the the $SU(2)_L \times U(1)_Y$ spontaneously breaks down leading to three massive bosons and one massless boson (photon).

2.2 Higgs Boson

2.2.1 The Higgs Mechanism

The Higgs Mechanism is a spontaneous symmetry breaking mechanism that results in the gauge bosons and fermions aquiring mass. For a real scalar field, the Lagrangian density can be written as in equation 1.

$$\mathcal{L} = \frac{1}{2}(\partial_\mu \phi)^2 - \frac{1}{2}\mu^2\phi^2 - \frac{1}{4}\lambda\phi^4 \tag{1}$$

This for a field of this form, it is possible to have a non-zero minimum if $\mu^2 < 0$. The ground state, or vacuum expectation value is shown in equation 2, and it can have two values.

$$\phi = \pm\sqrt{-\frac{\mu^2}{\lambda}} \tag{2}$$

The choice of one minima breaks the symmetry of the system regardless of the symmetry upon inversion of $\phi \to -\phi$. The field ϕ can be written in terms of a real scalar field h which is referred to as the Higgs boson. This boson couples more strongly to heavier particles, so it is these that are studied for its formation and decay.

2.2.2 Higgs Production

As this is a study at a linear collider, only certain processes contribute significantly to the production of a Higgs Boson. These processes are WW-fusion, Higgs Strahlung and ZZ-fusion and are shown in figures 1, 2 and 3. This is in contrast to experiments such as those at the LHC where the dominant production process is gluon fusion which produces Higgs Bosons through a top quark loop. Measurement of the total width of the Higgs Boson is not possible at the LHC as absolute values of the coupling constants are only attainable if the production and decay modes are the same. This is not the case at the LHC where only the ratios of the couplings are attainable. Therefore the total decay width and absolute values of couplings are measurements that are a unique feature of the ILC.

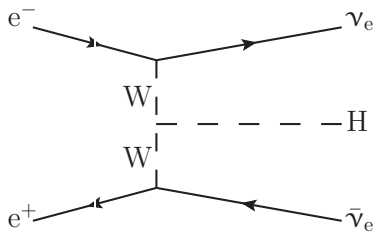

Figure 1: *Higgs Formation via WW Fusion*

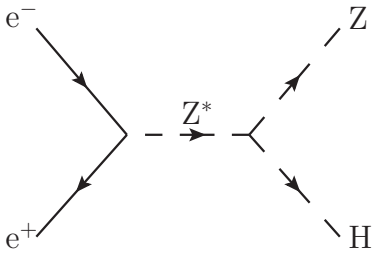

Figure 2: *Higgs Formation via Higgs Strahlung*

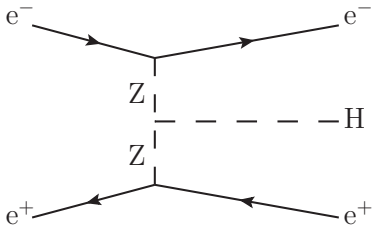

Figure 3: *Higgs Formation via ZZ Fusion*

The formation of the Higgs via ZZ fusion is suppressed due to the difference in the couplings as given by the electroweak mixing angle. Therefore the cross section for Higgs production is significantly lower and ignored for this analysis.

I have calculated the cross section for WW fusion and Higgs strahlung processes using a program called *Whizard* as a function of centre of mass energy. This is shown in figure 4. The cross section for WW fusion dominates over Higgs strahlung at the centre of mass energy I will be investigating. This is beneficial for this analysis as it means it will be easier to separate the two contributions. At lower centre of mass energy the two have a similar contribution.

These cross sections are calculated for two different beam polarisations. The beams of electrons and positrons produced in the ILC will be polarised with an efficiency of 80%

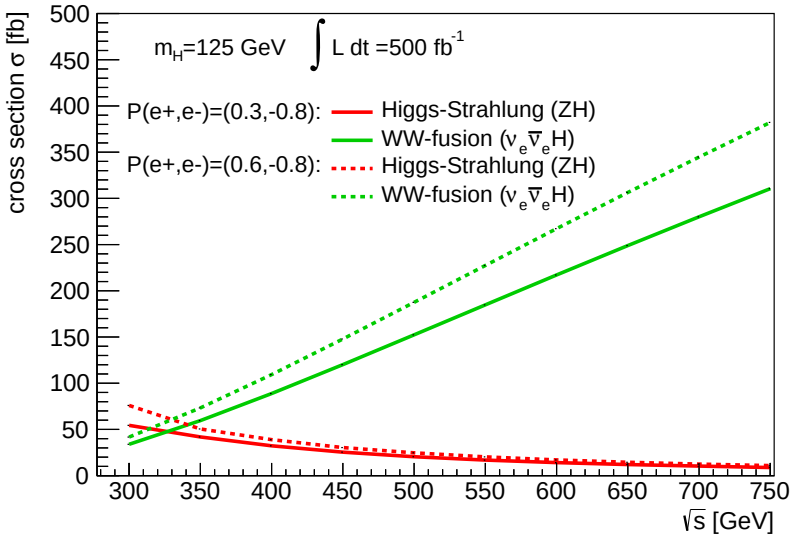

Figure 4: *Cross section for WW fusion and Higgs strahlung as a function of energy*

for the electrons and initially 30% for the positrons, then increased to 60%. These polarisation states labelled $P(e^+, e^-) = (0.3, -0.8)$ and $P(e^+, e^-) = (0.6, -0.8)$ can be used to calculate the overall cross section from the cross sections for the individual polarisations.

$$\sigma_{P(e^+,e^-)} = \left(\frac{1 - P_{e^-}}{2}\right)\left(\frac{1 + P_{e^+}}{2}\right)\sigma_{RL} + \left(\frac{1 + P_{e^-}}{2}\right)\left(\frac{1 - P_{e^+}}{2}\right)\sigma_{LR} \tag{3}$$

2.2.3 Total Width Determination

The total width of the Higgs Boson cannot be determined from the width of the resonance as the total width is significantly smaller than the resolution of the detector for light Higgs masses. From figure 5 you can see that for a Higgs mass of $m_H = 125\,\text{GeV}$ the total width is of the order of MeV.

It is possible to obtain the total width by an indirect method, however, by measuring just the cross section for WW fusion. This means this analysis will have to select only the signal events and remove all other processes that would have otherwise contributed to the total width.

To calculate the partial width of the Higgs, $\Gamma_{H\to WW}$, we take advantage of the fact that both $\Gamma_{H\to WW}$ and $\sigma_{wwfusion}$ depend on the square of the coupling constant, g^2_{HWW}. These processes are illustrated in figure 6.

In the limit of high energy $\sqrt{s} \gg 2m_w$ the approximate form of the cross section for WW fusion is shown in equation 4.

$$\sigma_{wwfusion} \to \frac{g^2_{HWW} G^2_F}{32\pi^3}\left[\left(1 + \frac{m^2_H}{s}\right)\log\left(\frac{s}{m^2_H}\right) - 2\left(1 - \frac{m^2_H}{s}\right)\right] \tag{4}$$

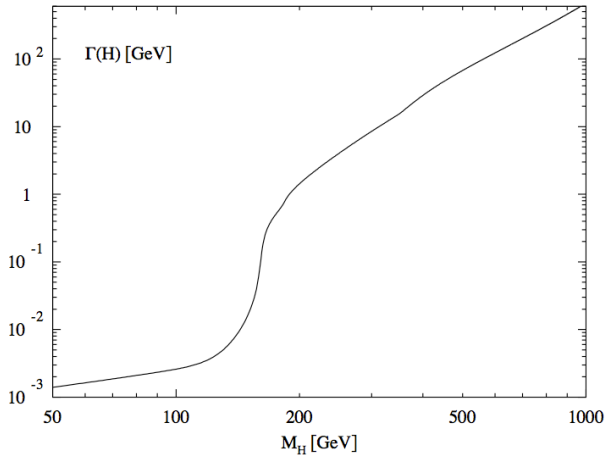

Figure 5: *The total decay width of the Higgs Boson as a function of Higgs mass*

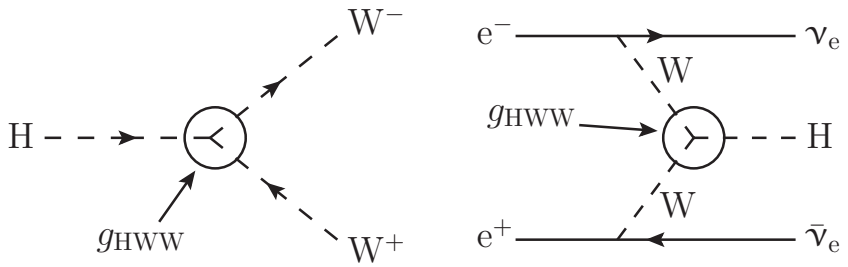

Figure 6: *Coupling constant for $H \rightarrow WW$ and WW fusion*

The partial width for the decay $H \rightarrow WW$ is given in equation 5.

$$\Gamma(H \rightarrow WW) = \frac{g_{HWW}^2 m_H^3}{64\pi m_W^3}\left(1 - \frac{4m_W^2}{m_H^2} + \frac{12m_W^4}{m_H^4}\right) \tag{5}$$

From here onwards we drop these constants of proportionality to write the relationship more concisely as shown in equation 6.

$$\Gamma(H \rightarrow WW) \propto g_{HWW}^2 \propto \sigma_{wwfusion} \tag{6}$$

The total decay width can be found by using the branching ratio for the decay to WW as shown in equation 7.

$$\Gamma_H^{tot} = \frac{\Gamma(H \rightarrow WW)}{BR(H \rightarrow WW)} \propto \frac{\sigma_{wwfusion}}{BR(H \rightarrow WW)} \tag{7}$$

Therefore by measuring the cross section for WW fusion the total decay width can be calculated assuming the branching ratio for a Higgs decaying to WW is known. This value must be determined from another analysis and will have an error associated with it [1].

2.2.4 Higgs Decay

The branching ratios for the Higgs to decay into different products changes as a function of its energy. For this analysis the Higgs mass is taken to be $m_H = 125\,\text{GeV}$. The larger Higgs masses couple more strongly to the heavier particles such as the Z and W boson as well a the t quark.

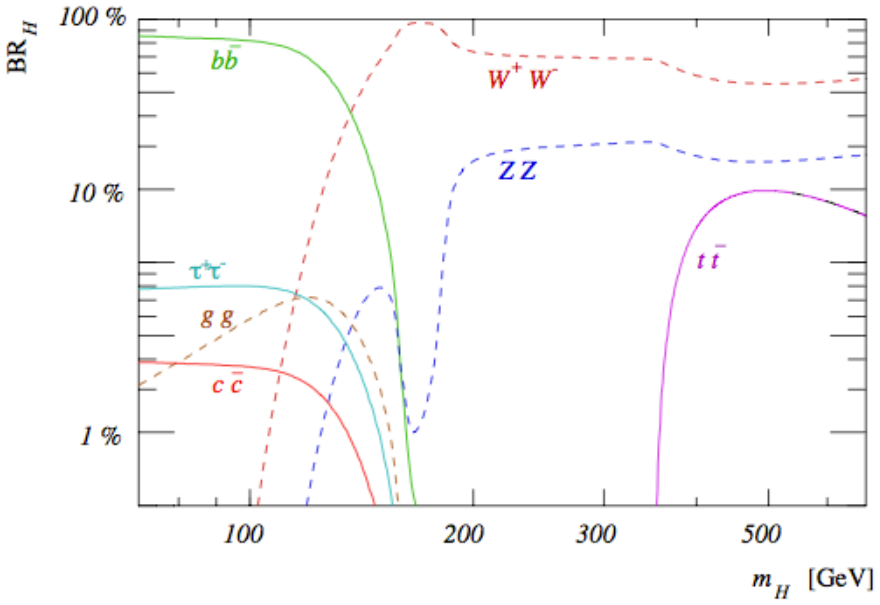

Figure 7: *Branching ratio of the Higgs Boson as a function of mass*

As you can see from figure 7 the dominant decay at the Higgs mass used is to $b\bar{b}$. For this analysis a b-tagging algorithm can be used to label jets as coming from a b quarks and hence a Higgs.

The cross section for WW fusion can be calculated from the number of WW fusion events and the luminosity as shown in equation 8.

$$\sigma_{WW\,fusion} = \frac{N_{WW}}{\mathcal{L}} \tag{8}$$

Here it must be noted that the sample of WW fusion events contains all of the decay products of the Higgs and the number of each were calculated using the standard model branching ratios. After the cuts not all of these WW fusion events will remain as some will be falsely removed by the selection so we need to replace the number of WW events,

N_{WW}, by the number measured, N'_{WW}. We can relate these two quantities using an efficiency shown in equation 9.

$$\epsilon = \frac{N'_{WW}}{N_{WW}} \tag{9}$$

As the sample of WW fusion events was created in a Monte Carlo that depends on the standard model branching ratios this efficiency will be a function of the $H \rightarrow b\bar{b}$ branching ratio. This is because we are looking in the sample only for the decays to $b\bar{b}$ and the number of these events that make it though the selection process is dependent on the value of $BR(H \rightarrow b\bar{b})$ chosen for the Monte Carlo simulation.

3 Signal and Background Processes

3.1 Signal Processes

The signal process for this simulation is the formation of a Higgs via WW fusion which then decays into a $b\bar{b}$ pair. This is shown in equation 10.

$$e^+e^- \rightarrow H\nu_e\bar{\nu_e} \rightarrow b\bar{b}\nu_e\bar{\nu_e} \tag{10}$$

This process can be characterised by a large missing energy due to the neutrino pair going undetected. The two b quarks will also hardonise to form jets in the calorimeter. These jets can be identified by b-tagging algorithms as coming from b quarks due to their unique characteristics.

3.2 Background Processes

There are a selection of background processes that need to be taken into account and reduced as much as possible by the event selection so as to reduce the error on the total width.

The background processes that I have taken into account in this analysis are listed in table 3 along with the number of events that I need to take into account. These are originally obtained for the individual polarisations but then combined to make a single number by using equation 3 so that the expected background is appropriate for the polarisation used in our simulation.

There are some background processes that haven't been included in this analysis that should be added to further studies. The first of these is the leptonic decay of two Z bosons: $ZZ \rightarrow l\bar{l}$. This process should be reduced fairly effectively by the isolated lepton removal cut and not cause much to change. The second is the mixing contribution for the states that could come from either $ZZ \rightarrow q\bar{q}q\bar{q}$ or $W^+W^- \rightarrow q\bar{q}q\bar{q}$ for example $uddu$ or $cssc$ states. The third is the contribution to the six fermion background from $t\bar{t}$ samples. This is important because the top quarks decay to b quarks and produce similar products to our signal.

Type	**Decay**	N_{events}
Semileptonic	$W^+W^- \to \nu_\ell \ell^\pm q\bar{q}$	2,785,120
Hadronic	$W^+W^- \to q\bar{q}q\bar{q}$	2,245,500
Semileptonic	$ZZ \to \ell\bar{\ell}q\bar{q}$	182,999
Hadronic	$ZZ \to q\bar{q}q\bar{q}$	203,310
Semileptonic	$W^\mp e^\pm \nu_e \to e^\pm \nu_e q\bar{q}$	2,283,520
Semileptonic	$Ze^+e^- \to q\bar{q}e^-e^+$	603,845
Hadronic	$Z \to q\bar{q}$	9,805,180
Semileptonic	$Z\nu\bar{\nu} \to q\bar{q}\nu\bar{\nu}$	279,408

Table 3: *Background processes and expected numbers of events for* $\sqrt{s} = 500\ GeV$ *and* $\mathcal{L} = 500\ fb^{-1}$

The largest contribution to the background is the hadronic decay of the Z boson, but this easily removable because it has different characteristics to the signal process.

The simulation I have used in this analysis uses the full simulation of the *International Large Detector* (ILD), details of this detector can be found in the Technical Design Report [2].

4 Determination of Total Decay Width Precision

4.1 Event Selection and Cuts

In order to separate the signal events from the total events I applied cuts to the data on variables that had discriminating characteristics. These cuts are listed in table 4 and show the range over which the variable must be within to be kept in the analysis. These cuts are on similar parameters to the earlier fast simulation [3] but the exact cut values have been optimised to get better results.

I will define and illustrate the effect of some of these cuts on my signal and background samples in this section.

Initially an algorithm is run on the sample to identify the number of isolated leptons in the sample. The first cut that is implemented is to remove any events with two or more isolated leptons. This helps to remove leptonic background events.

4.1.1 Visible Mass

The visible mass is defined as the invariant mass made out of the visible energy and the visible momentum as shown in equation 11. Here the visible energy is the sum of all the energy deposited in the detector and the visible momentum is the sum of all the

Name	Cut
Isolated lepton removal	No. isolated lep ≤ 1
Visible mass	$105\,\text{GeV} \leq m_{vis} \leq 135\,\text{GeV}$
Visible energy	$105\,\text{GeV} \leq E_{vis} \leq 255\,\text{GeV}$
Visible P_t	$5\,\text{GeV} \leq \sum P_T \leq 200\,\text{GeV}$
Polar angle of jet	$\lvert\cos\theta_{Jet}\rvert \leq 0.9$
Angle between jets	$\cos\alpha \leq 0.2$
Acoplanarity	Acop ≥ 10
Durham, Y_{12} (minus)	$0.2 \leq Y_{12} \leq 0.8$
b-tagging	b-tag ≥ 0.5
Number of tracks	$10 \leq N \leq 60$

Table 4: *Summary of cuts performed*

momentum observed in the detector.

$$m_{vis} = \sqrt{E_{vis}^2 - |\mathbf{p}_{vis}^2|} \tag{11}$$

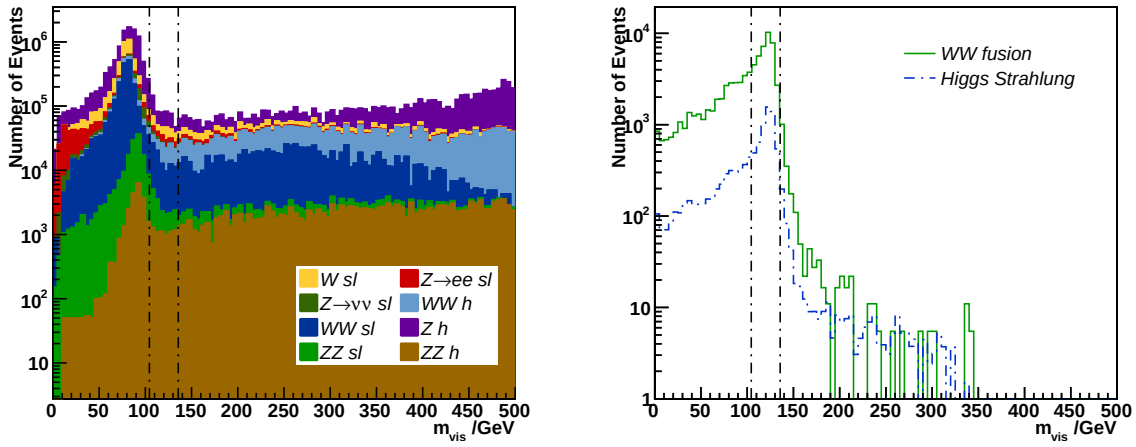

Figure 8: *Plot showing the distribution of m_{vis} for (1) background and (2) WW fusion and Higgs strahlung before any cuts are applied (h = hadronic, sl = semileptonic)*

Figure 8 shows the distribution of the visible mass for background, WW fusion and Higgs strahlung events. The dotted vertical lines illustrate where the cuts are taken on the visible mass. This cut keeps events that are within the range $m_H - 20\,\text{GeV} \leq m_{vis} \leq m_H + 10\,\text{GeV}$ as the signal and Higgs strahlung events have a peak at the Higgs mass. The background has a peak at lower masses, nearer the W and Z mass, so this removes a large amount of background.

4.1.2 Visible Energy

The visible energy is the sum of the individual energies for particles in the reconstruction. The distribution is different for the different samples as shown in figure 9.

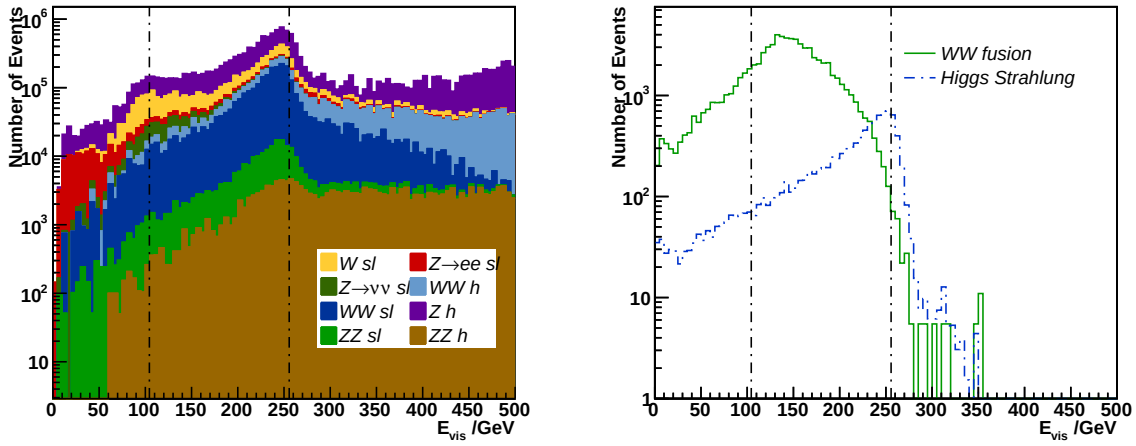

Figure 9: *Plot showing the distribution of E_{vis} for (1) background and (2) WW fusion and Higgs strahlung before any cuts are applied (h = hadronic, sl = semileptonic)*

In this case the signal and Higgs strahlung distributions peak at different values. This cut is chosen so as to retain the majority of the signal whilst removing a large amount of background at higher energies.

4.1.3 Transverse Momentum

The transverse momentum is the sum of the visible momentum in the plane perpendicular to the beam direction.

Events with a total transverse momentum in the range 5 GeV$\leq \sum P_T \leq$ 200 GeV are kept in this analysis. You can see from the distribution in figure 10 that WW fusion and Higgs strahlung peak at different values, so the cut on this variable can remove some background and Higgs strahlung without affecting the signal significantly.

4.1.4 Acoplanarity

The acoplanarity is defined as the angle between the two jets when they are projected onto the plane perpendicular to the beam direction. In this analysis it is required to be larger than 10° which removes background as this has a peak at low acoplanarity angles.

The distribution is shown in figure 11.

4.1.5 Durham Y_{12}

The events in each sample are forced into two jets by a jet finding algorithm called the Durham Algorithm. The Durham parameter Y_{12} or Y_{-} gives the likelihood that the two

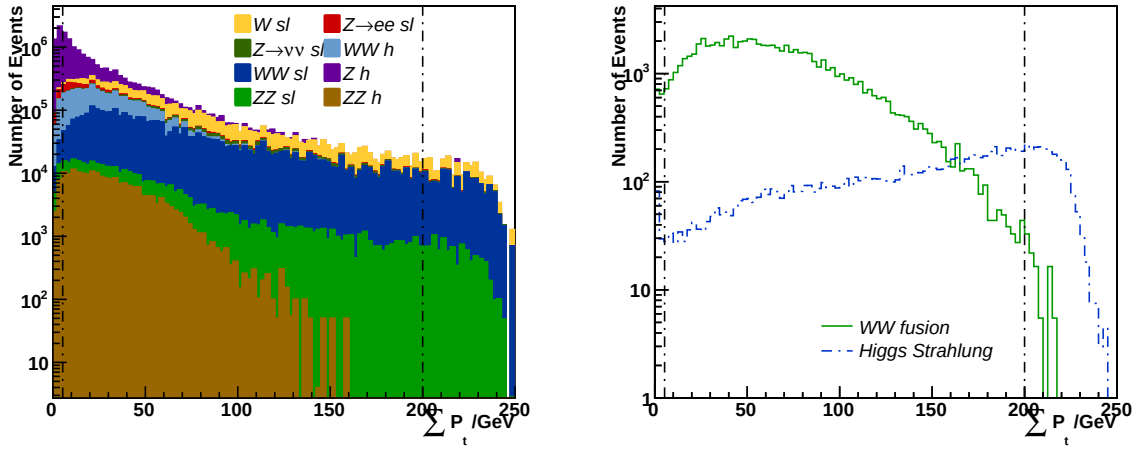

Figure 10: *Plot showing the distribution of $\sum P_t$ for (1) background and (2) WW fusion and Higgs Strahlung before any cuts are applied (h = hadronic, sl = semileptonic)*

jets identified are actually one jet. This is a useful parameter to remove background as many backgrounds have a high likelihood that they came from one jet where as for both WW fusion and Higgs strahlung there are few events with low Y_{12}.

There is also a peak for the signal at very low Y_{12} so there is two cuts on this parameter to keep the range $0.2 \leq Y_{12} \leq 0.8$. This is shown in figure 12.

4.1.6 b-tagging

In this investigation I have used a b-tagging algorithm to identify events that originate from the decay of b quarks. This is an important parameter and helps to remove background events. As there are two jets in each event, I require that both of them pass the cut condition in order to kept. The distribution of this parameter is shown in figure 13.

From this plot you can see that there is a peak for all of the samples at low and high b-tag values. The peak for WW fusion events around one is higher with respect to the lower peak than for the other samples indicating it is useful for removing both background and Higgs Strahlung events.

4.1.7 Polar Angle of Jet θ_{jet}

The polar angle of the jet is defined as the angle between the jet and the beam axis. The cut in my analysis requires that for both jets $|\cos\theta_{jet}| \leq 0.9$ and this helps to reduce the number of background events as these peak at high $|\cos\theta_{jet}|$ values where as the signal and Higgs strahlung don't to the same extent. This effect is shown in figure 14.

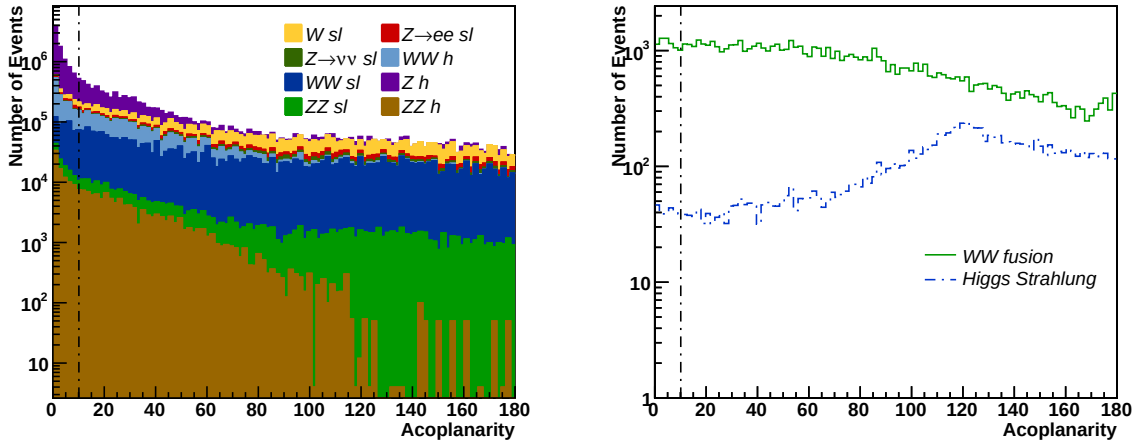

Figure 11: *Plot showing the distribution of the Acoplanarity for (1) background and (2) WW fusion and Higgs strahlung before any cuts are applied (h = hadronic, sl = semileptonic)*

4.1.8 Angle Between Jets

The angle between the jets is called α and is a useful parameter to remove both background and Higgs strahlung. The distribution of this variable is shown in figure 15.

From this figure you can see that there is a peak for the background at around $\cos\alpha \approx 0.8$ and for Higgs strahlung at around $\cos\alpha \approx 0.6$ where as no peak exists for the signal. This means this cut effectively reduces the contribution from these events.

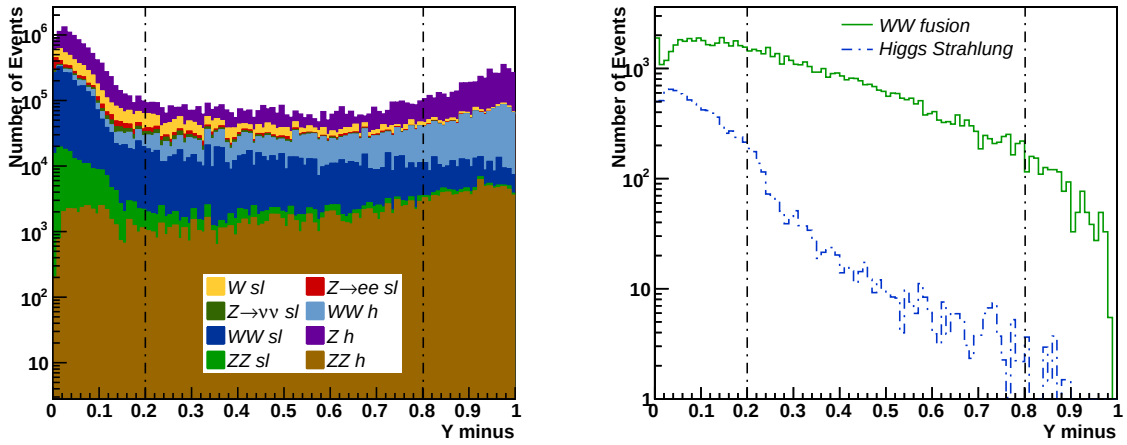

Figure 12: *Plot showing the distribution of the Durham parameter Y_{12} for (1) background and (2) WW fusion and Higgs strahlung before any cuts are applied (h = hadronic, sl = semileptonic)*

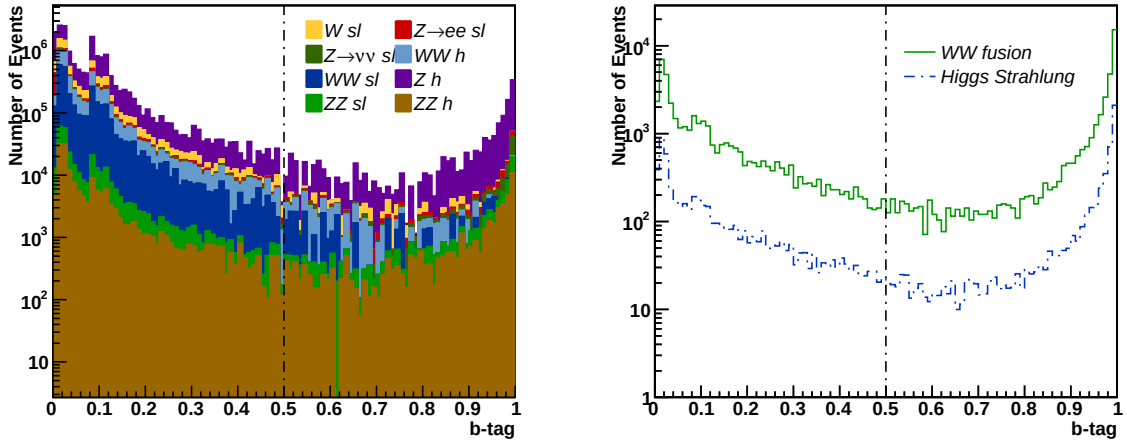

Figure 13: *Plot showing the distribution of both b-tags for (1) background and (2) WW fusion and Higgs Strahlung before any cuts are applied (h = hadronic, sl = semileptonic)*

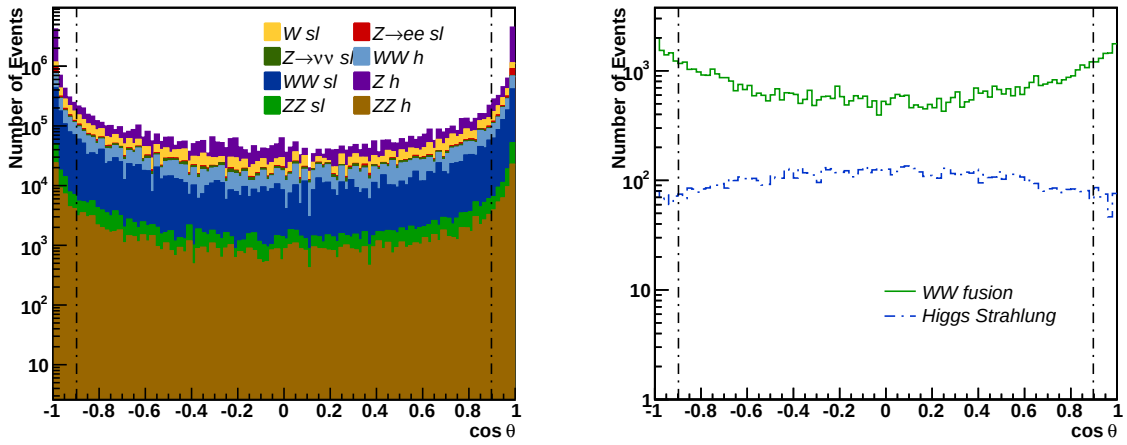

Figure 14: *Plot showing the distribution of* $\cos\theta_{jet}$ *for (1) background and (2) WW fusion and Higgs strahlung before any cuts are applied (h = hadronic, sl = semileptonic)*

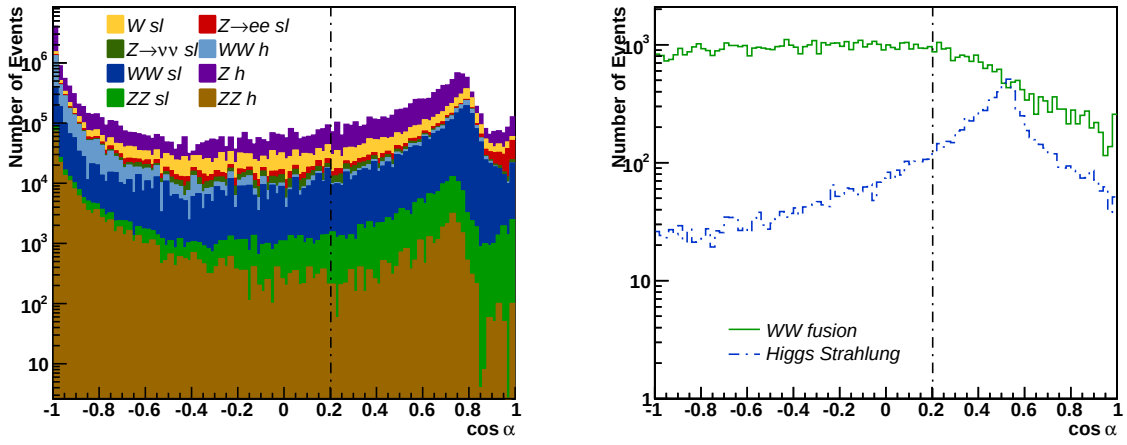

Figure 15: *Plot showing the distribution* $\cos\alpha$ *for (1) background and (2) WW fusion and Higgs strahlung before any cuts are applied (h = hadronic, sl = semileptonic)*

4.2 Effect of Cuts

The effect of the cuts acting sequentially on the data samples is shown in table 5.

Cut	**Background**	**WW fusion**	**Higgs strahlung**
No cut	18,388,882	76,161	10,222
Isolated Leptons	18,152,821	74,427	10,005
Visible Mass	513,784	37,521	5,638
Visible Energy	349,310	37,424	4,534
Transverse Momentum	295,609	37,215	3,554
Polar angle of jets	108,079	29,958	3,279
Angle between jets	92,302	25,919	1,037
Acoplanarity	85,280	24,071	987
Durham Y_{12} (minus)	48,053	16,596	243
b-tag	447	8,460	112
No. of Tracks	**308**	**8,103**	**107**

Table 5: *Effect of the cuts on the samples*

We end up with a much smaller number of both background events and Higgs strahlung events, whilst retaining a significantly bigger fraction of the WW fusion.

In order to distinguish between the Higgs strahlung and WW fusion samples it is useful to look at a parameter called the missing mass. It is defined as the invariant mass made out of the missing energy and missing momentum as defined in equation 12.

$$m_{mis} = \sqrt{E_{mis}^2 - |\mathbf{p}_{mis}^2|} \tag{12}$$

Here the missing energy and missing momentum are defined as in equations 13 and 14

$$\mathbf{p}_{mis} = -\mathbf{p}_{vis} \tag{13}$$

$$E_{mis} = \sqrt{s} - E_{vis} \tag{14}$$

We expect different characteristics for the missing mass due to the invariant mass of the $\nu\bar{\nu}$ pair. In Higgs strahlung we would expect $m_{mis} \approx m_Z$ where as in WW fusion it would be much higher as $\nu\bar{\nu}$ are not constrained to be the decay product of a Z boson.

In figure 16 the distribution of m_{mis} is shown for the sample before any cuts are performed. This shows the difference in the location of the peak for WW fusion and Higgs strahlung as expected.

Figure 17 shows the distribution of m_{mis} after all of the cuts have been applied.

This figure shows a significantly reduced number of background and Higgs strahlung events, with a relatively large WW fusion signal.

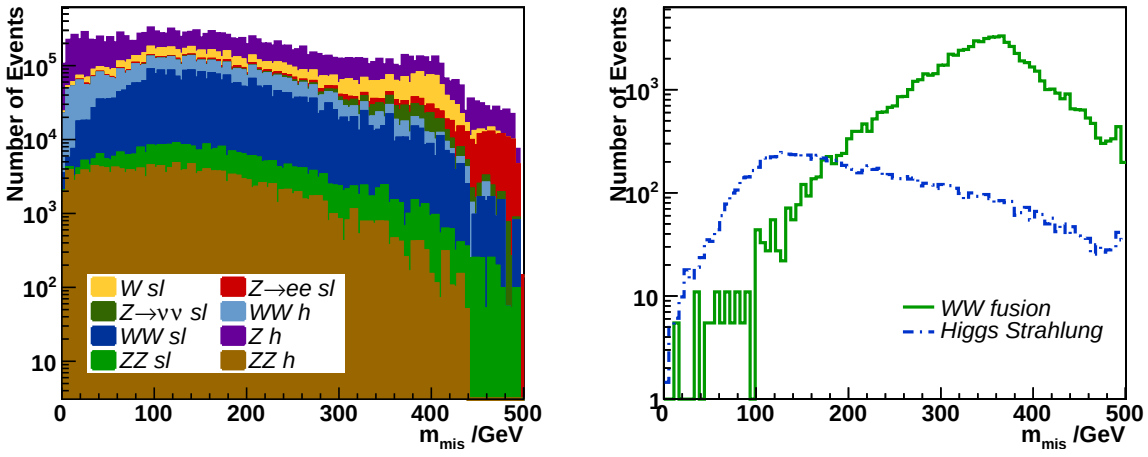

Figure 16: *Plot showing the distribution of m_{mis} for (1) background and (2) WW fusion and Higgs Strahlung before any cuts are applied (h = hadronic, sl = semileptonic)*

This plot also has two more data sets plotted that are used to determine the uncertainty on the number of signal and background events. The first is a toy Monte Carlo simulation represented by the points. This has been generated using part of the *root* package called *RooFit*. This has been used to create a probability distribution function (PDF) out of the total distribution. Next, these events were generated using this PDF to give the points shown.

The second new data set is the fit shown in green. For this the *root* package *TMinuit* was used to create a model to be fitted to the MC toy data. The following function shown in equation 15 was created.

$$N_{pred,i} = f_{WW} N_{WW,i} + f_{ZH} N_{ZH,i} + f_{BG} N_{BG,i} \tag{15}$$

Here $N_{WW,i}$ is the number of WW events in the ith bin and the same for $N_{ZH,i}$ and $N_{BG,i}$ respectively. The parameters f_{WW}, f_{ZH} and f_{BG} are adjusted by *TMinuit* so as to minimise the χ^2 function given in equation 16.

$$\chi^2 = \sum_{i}^{Nbins} \left(\frac{N_{data,i} - N_{pred,i}}{\sigma_{data,i}} \right)^2 \tag{16}$$

This minimisation resulted in fitted values for the number of each type of event along with their associated errors.

Process	No. of Events
WW Fusion	8049 ± 160
Higgs Strahlung	101 ± 124
Background	340 ± 39

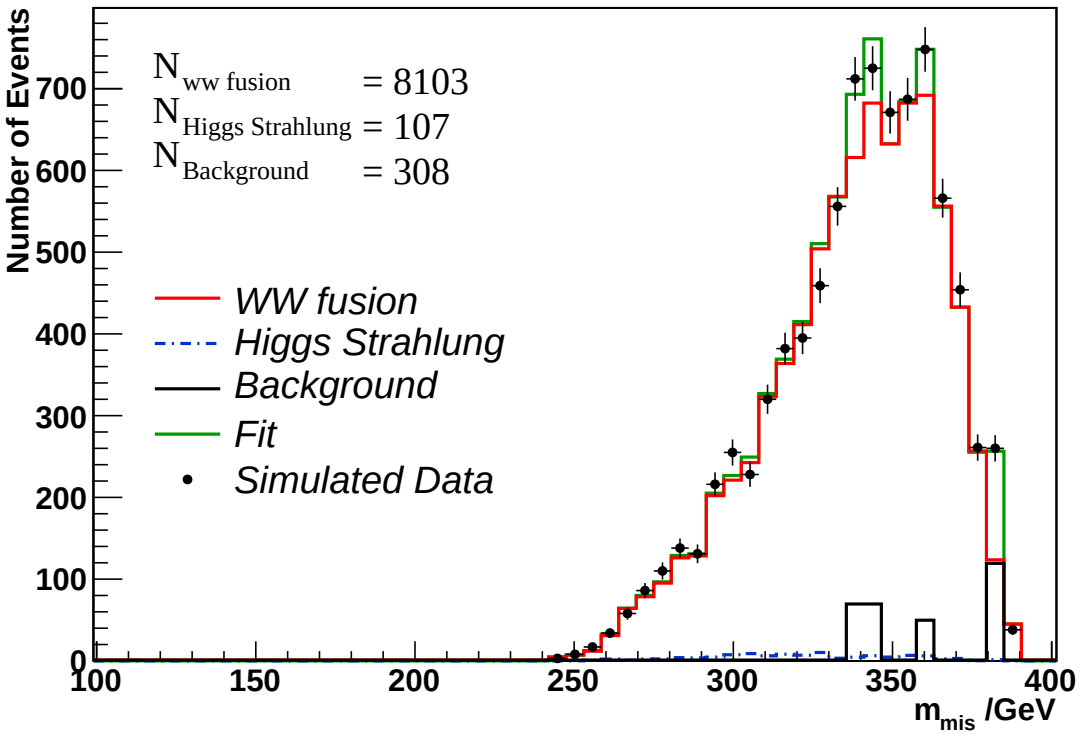

Figure 17: *Plot showing the distribution of m_{mis} for background, WW fusion and Higgs strahlung along with MC toy data and a fit*

From this we can deduce that the overall uncertainty in the number of WW fusion events is given by

$$\left(\frac{\Delta N'_{WW}}{N'_{WW}}\right) = 1.99\% \tag{17}$$

We can compare this distribution to the previous fast simulation also at a centre of mass energy of 500 GeV but with a lower Higgs mass of $m_H = 120\,\text{GeV}$ and this is shown in figure 18. I have replotted the fit from my simulation alongside in figure 19 for comparison.

These two figures show that the plots have the same overall shape with a large number of WW fusion events and relatively small background and Higgs strahlung contributions. The full simulation plot has no events below about 250 GeV which is a result of the cut on the parameter Y_{12}. This cut is effective at removing the background events but also removes some signal too. This is in contrast to the previous fast simulation which didn't use this parameter, opting instead for Y_{23} which give the likelihood that the event actually had three jets not two. Other factors that might explain the difference in the appearance is that the previous simulation was carried out in 2000, 13 years before this one, and it

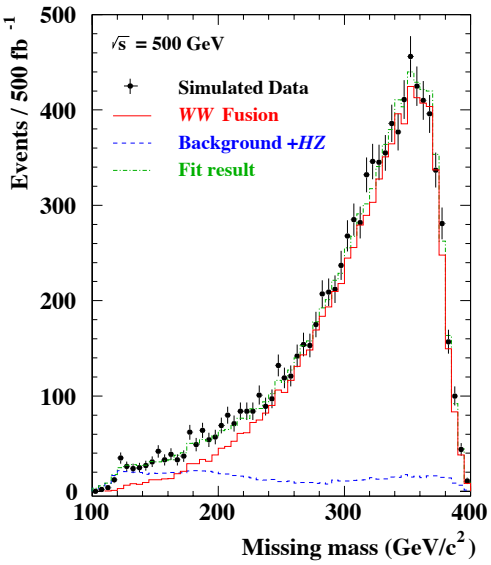

Figure 18: *Fast Simulation*

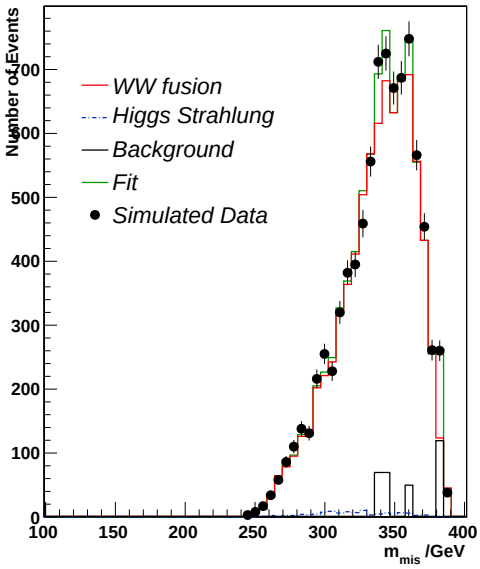

Figure 19: *Full Simulation*

was modelled on a different detector. Taking this into account, the results of the fits are compared in the table below and are fairly consistent with exception of the lower number of Higgs strahlung events in the full simulation, and slightly larger uncertainties.

Process	Fast Simulation	Full Simulation
WW Fusion	8181 ± 98	8049 ± 160
Higgs Strahlung	229 ± 21	101 ± 124
Background	348 ± 38	340 ± 39

4.3 Determining the Precision of the Total Decay Width

4.3.1 Error Propagation

The relationship between the Higgs total decay width and the WW fusion cross section is shown again below in equation 18, and the relationship between the WW fusion cross section and the number of WW fusion events is shown in equation 19.

$$\Gamma_H^{tot} = \frac{\Gamma(H \to WW)}{BR(H \to WW)} \propto \frac{\sigma_{WW\,fusion}}{BR(H \to WW)} \tag{18}$$

$$\sigma_{WW\,fusion} = \frac{N'_{WW}}{\epsilon \cdot \mathcal{L}} \tag{19}$$

If we assume there is no error associated with the luminosity, $\mathcal{L}$, but that the efficiency is a function of the branching ratio $BR(H \to b\bar{b})$ then we can write the error in these two values as follows in equation 20 and 21

$$\left(\frac{\Delta\sigma_{WW\,fusion}}{\sigma_{WW\,fusion}}\right)^2 = \left(\frac{\Delta N'_{WW}}{N'_{WW}}\right)^2 + \left(\frac{\Delta BR(H \to b\bar{b})}{BR(H \to b\bar{b})}\right)^2 \tag{20}$$

$$\left(\frac{\Delta\Gamma_H^{tot}}{\Gamma_H^{tot}}\right)^2 = \left(\frac{\Delta\sigma_{WW}}{\sigma_{WW}}\right)^2 + \left(\frac{\Delta BR(H \to WW)}{BR(H \to WW)}\right)^2 \tag{21}$$

4.3.2 Obtaining Uncertainty

From the fit we obtain an estimate of the error on the number of WW fusion events.

$$\left(\frac{\Delta N'_{WW}}{N'_{WW}}\right) = 1.99\% \tag{22}$$

It is useful to compare this value to the previous fast simulation [3]. For a Higgs mass of $m_H = 120\,\text{GeV}$ an uncertainty of $\left(\frac{\Delta N'_{WW}}{N'_{WW}}\right) = 1.2\%$ was obtained and for $m_H = 130\,\text{GeV}$ an uncertainty of $\left(\frac{\Delta N'_{WW}}{N'_{WW}}\right) = 2.4\%$ was obtained. The result from this analysis is slightly larger than the value you would expect by simply extrapolating between these two values. A possible reason for this could be due to the difference in shapes of the missing mass distribution shown in figures 18 and 19. The current full simulation has a similar shape distribution for the Higgs strahlung and WW fusion samples where as they have different shapes in the previous fast simulation. This means when the fit is conducted for the full simulation there is a fairly big margin either side to add different fractions of the WW fusion or Higgs strahlung where as this is much narrower in the fast simulation case.

From other investigations we obtain two different sets of uncertainties on the branching ratios depending on how much data has been collected[1]. When the ILC has collected 500 fb^{-1} of data at $\sqrt{s} = 500$ GeV we get the values called the *ILC(500) baseline* values which are as follows.

$$\left(\frac{\Delta BR(H \to b\bar{b})}{BR(H \to b\bar{b})}\right) = 3.6\%, \left(\frac{\Delta BR(H \to WW)}{BR(H \to WW)}\right) = 2.8\% \tag{23}$$

We can also obtain the "ultimate" uncertainties which are given for when the ILC has been running at $\sqrt{s} = 1\,\text{TeV}$ and collected 1000 fb^{-1} of data. This is called the *ILC(1000) LumUp* value and are as follows.

$$\left(\frac{\Delta BR(H \to b\bar{b})}{BR(H \to b\bar{b})}\right) = 1.48\%, \left(\frac{\Delta BR(H \to WW)}{BR(H \to WW)}\right) = 1.3\% \tag{24}$$

Using these "ultimate" values we find that the error on the cross section for WW fusion is

$$\left(\frac{\Delta\sigma_{WW\,fusion}}{\sigma_{WW\,fusion}}\right) = 2.48\% \tag{25}$$

And the uncertainty on the measurement of the total decay width of the Higgs Boson is

$$\left(\frac{\Delta\Gamma_H^{tot}}{\Gamma_H^{tot}}\right) = 2.8\% \tag{26}$$

5 Conclusions

To summarise I have conducted a full simulation of the total decay width of the Higgs Boson at the ILC for a centre of mass energy of $\sqrt{s} = 500$ GeV and luminosity of $\mathcal{L} = 500$ fb^{-1} . This was made possible by an indirectly method as the decay width would be too small to resolve with the ILC. The signal process was chosen to be WW fusion as the cross section for this is proportional to the partial decay width for $H \to WW$ due to their shared dependence on the coupling constant g_{HWW}. I used a range of cuts on the data sets to remove background events and Higgs strahlung events that also produce Higgs Bosons. The decay of the Higgs to $b\bar{b}$ was used as it is dominant at $m_H = 125\,\text{GeV}$ and a b-tagging algorithm was used to identify jets coming from b quarks.

I used the distribution of the missing mass m_{mis} to create a toy Monte Carlo dataset which was then used to fit back to the original distributions in order to minimise a χ^2 function. The resulting error in the number of WW fusion events from this fit was propagated using the expected uncertainties in the branching ratios to establish the uncertainty in the total decay width. This uncertainty was established to be $\left(\frac{\Delta\Gamma_H^{tot}}{\Gamma_H^{tot}}\right) = 2.8\%$ which is consistent and slightly smaller than the previous fast simulation into the TESLA detector[3].

References

[1] **ILC** Higgs Whitepaper for Snowmass Community Study 2013
https://indico.fnal.gov/getFile.py/access?contribId=387&sessionId=77&resId=1&materialId=slides&confId=6890

[2] **ILC** Technical Design Report *Volume 4 -Detectors*; Part III

[3] **Niels Meyer** Higgs-Bosons At TESLA: Studies On Production In WW-Fusion And Total Decay Width *Universität Hamburg*; Juli 2000